Published in final edited form as:

Channels (Austin). 2009 ; 3(1): 57–68. doi:10.4161/chan.3.1.7817.

The Kir channel immunoglobulin domain is essential for Kir1.1 (ROMK) thermodynamic stability, trafficking and gating

Katherine Fallen[1,†], **Sreedatta Banerjee**[1,†], **Jonathan Sheehan**[4], **Daniel Addison**[1], **L. Michelle Lewis**[5], **Jens Meiler**[2,4,6], **Jerod S. Denton**[1,2,3,*]

[1]Department of Anesthesiology, Vanderbilt University Medical Center; Nashville, TN USA

[2]Department of Pharmacology, Vanderbilt University Medical Center; Nashville, TN USA

[3]Digestive Disease Research Center, Vanderbilt University Medical Center; Nashville, TN USA

[4]Center for Structural Biology, Vanderbilt University Medical Center; Nashville, TN USA

[5]Institute for Chemical Biology, Vanderbilt University Medical Center; Nashville, TN USA

[6]Department of Chemistry, Vanderbilt University Medical Center; Nashville, TN USA

Abstract

The renal inward rectifying potassium channel Kir1.1 plays key roles in regulating electrolyte homeostasis and blood pressure. Loss-of-function mutations in the channel cause a life-threatening salt and water balance disorder in infants called antenatal Bartter syndrome (ABS). Of more than 30 ABS mutations identified, approximately half are located in the intracellular domain of the channel. The mechanisms underlying channel dysfunction for most of these mutations are unknown. By mapping intracellular mutations onto an atomic model of Kir1.1, we found that several of these are localized to a phylogenetically ancient immunoglobulin (Ig)-like domain (IgLD) that has not been characterized previously, prompting us to examine this structure in detail. The IgLD is assembled from two β-pleated sheets packed face-to-face, creating a β-sheet interface or core, populated by highly conserved side chains. Thermodynamic calculations on computationally mutated chan-nels suggest that IgLD core residues are among the most important residues for determining cytoplasmic domain stability. Consistent with this notion, we show that two ABS mutations (A198T and Y314C) located within the IgLD core impair channel biosynthesis and trafficking in mammalian cells. A fraction of core mutant channels reach the cell surface, but are electrically silent due to closure of the helix-bundle gate. Compensatory mutation-induced rescue of channel function revealed that IgLD core mutants fail to rectify. Our study sheds new light on the pathogenesis of ABS and establishes the IgLD as an essential structure within the Kir channel family.

Keywords

inward rectifying potassium channel; trafficking; KCNJ1; thermodynamics; molecular modeling; Bartter syndrome; gating; immunoglobulin domain

*Correspondence to: Jerod S. Denton; Vanderbilt University Medical Center; B4220 Medical Center North; 1161 21st Avenue South; Nashville, TN 37232 USA; jerod.denton@vanderbilt.edu.

†These authors contributed equally to this work.

Introduction

Kir1.1 or ROMK (Renal Outer Medullary K^+ channel) is the founding member of the inward rectifier family of K^+ channels.[1–4] Kir1.1 is expressed widely in the kidney tubule where it plays essential and well-defined roles in regulating systemic fluid and electrolyte balance (reviewed in refs. 5 and 6). Heritable mutations in the gene encoding Kir1.1 (i.e., *KCNJ1*) cause antenatal Bartter syndrome (ABS), a life-threatening autosomal recessive disease presenting with polyhydramnios, polyuria, hypokalemic metabolic alkalosis and low to normal blood pressure.[7,8] To date more than 30 unique loss-of-function missense mutations in *KCNJ1* have been identified in ABS patients. However, the molecular and cellular mechanisms underlying loss of mutant channel function are not well understood. This represents a fundamental gap in our understanding of Kir channel biology and a critical barrier to development of channel-directed therapies for ABS.

Inward rectifying K^+ channels are oligomeric protein complexes containing four identical or similar subunits surrounding a central water-filled pore.[9,10] Each subunit contains a short intracellular alpha-helix (M0) preceding two transmembrane helices (M1 and M2), an extracellular pore loop and an extensive intracellular domain comprised of amino (N) and carboxyl (C) termini. Rectification is caused by voltage-dependent block of outward K^+ conduction by intracellular Mg^{2+} or polyamines.[11–13] The strength of rectification varies widely among family members, but generally reflects the number and spatial distribution of blocker binding sites lining the conduction pathway.[14–16] In comparison to some Kir channels, Kir1.1 is a characteristically weak inward rectifier.

Kir1.1 channel gating is critically regulated by intracellular pH (pH_i) and membrane phospholipids such as phosphatidylinositol 4,5-bisphosphate (PIP_2).[17–21] The wild-type (WT) channel exhibits a high open-state probability near physiological pH_i that decreases sharply upon intracellular acidification or disruption of PIP_2-channel interactions. The pH_i-open probability relationship yields an apparent acid dissociation constant (pK_a) near neutral pH. Protons and PIP_2 interact with distinct channel structures, but appear to act through a common gate located at the M1-M2 helix-bundle crossing near the membrane-cytosol interface.[9,22–25] Structural and functional data support a model in which lateral displacement of the transmembrane helices away from the pore axis mediates channel opening. Rapedius et al.[22,23] proposed that an intra-subunit hydrogen bond between lysine 80 (K80) and alanine 177 (A177) at the helix-bundle crossing stabilizes the closed state of the channel.[22,23] Mutation of K80 to methionine (K80M), which presumably disrupts the K80-A177 hydrogen bond, renders the channel refractory to closure by low pH_i,[18,21,26–28] and dramatically speeds the rate of channel activation by PIP_2.[22] A growing body of structural evidence suggests that conformational gating motions also occur within the deeper cytoplasmic domain of the channel.[10,24] The precise nature of these molecular motions and whether they are obligatorily coupled to gating at the helix-bundle crossing is not known.

Approximately half of the missense mutations identified in ABS patients occur in the cytoplasmic domain, and at least 6 of these (C49Y, I51T, D74Y, S219R, L220F, R311W/Q) are known shift the pK_a of the channel in the alkaline direction. As a consequence, channel

open probability at physiological pH_i is reduced, leading to loss of channel function and derangement of kidney tubule function.[26,45,46] Hebert and colleagues showed that the function of the R311Q mutant could be rescued by the second-site K80M mutation, indicating that the loss of function in this mutant channel is due at least in part to closure of the helix-bundle gate.[28] The mechanisms by which cytoplasmic domain mutations alter gating at the helix-bundle crossing are virtually unexplored, but are clearly relevant to the pathogenesis of ABS.

By mapping intracellular mutations onto an atomic model of Kir1.1, we found that several of these are localized to a phylogenetically ancient immunoglobulin (Ig)-like domain (IgLD) that has not been characterized previously, prompting us to examine this structure in detail. Using computational mutagenesis combined with conventional biochemical and electrophysiological approaches we show that thermodynamically destabilizing mutations within the core impair Kir1.1 channel biogenesis, trafficking and gating at the helix-bundle crossing. Furthermore, core mutations abolish Mg^{2+}-dependent current rectification, suggesting the IgLD helps maintain the native structure of the channel pore. Our study provides new insights into the molecular and cellular mechanisms of Kir1.1 channel dysfunction in ABS and establishes the IgLD as an essential structure within the Kir channel family.

Results

Structural features of the Kir channel immunoglobulin-like domain.

Recently available X-ray structures of bacterial and mammalian Kir channel proteins revealed that the structure of the cytoplasmic domain is highly conserved from bacteria to mice.[9,10,14,29,30] We noted that each Kir channel subunit harbored a β-sandwich structure resembling an immunoglobulin (Ig) domain, which is found in numerous structurally and functionally divergent proteins. To determine if this structure is a bona fide member of the Ig domain superfamily, the rat Kir1.1 sequence was submitted for fold recognition using the metaserver at http://meta.bioinfo.pl.[31] The best 20 resulting models (3D-Jury scores 141–195) were derived from closely related templates that are members of the “E set domains” superfamily (Structural Classification of Proteins classification b.1.18; http://scop.mrc-lmb.cam.ac.uk/scop).[32] This represents a subclassification of the Ig-like domain (IgLD) fold. Within the potassium channel superfamily, the E-set IgLD is limited to members of the Kir channel family, indicating this conserved fold is a unique and defining structural element of the inward rectifying K^+ channel family.

Figure 1A shows a homology model of the Kir1.1 cytoplasmic domain based on the X-ray structure of Kir3.1 (PDB code 2QKS).[10] The membrane-spanning portion illustrated in gray is that of a Kir3.1-KirBac1.3 chimera constructed by Nishida et al.[29] (PDB code 2QKS; see Methods). The cytoplasmic portion of each subunit is indicated with a different color. The IgLD of the green subunit (dashed box) is shown in Figure 1B isolated from the rest of the channel to highlight its geometry. The β-sandwich is assembled from two anti-parallel β-pleated sheets packed face-to-face. The β-sheets, which we term β_1 and β_2, are comprised of strands B, B’, C, G (Fig. 1B, left) and D, E, H, I (Fig. 1B, right), respectively. This β-strand nomenclature was adopted from Pegan et al.[14] β_1 and β_2 are rotated relative to one another

by approximately 30° to facilitate side chain packing between sheets, a characteristic feature of β-sandwich domains.[33] The interface between sheets, or core, is populated by hydrophobic side chains. Hydrophobic cores typically contain one or two aromatic residues surrounded by simple or branched hydrophobic side chains.[34,35] As shown in Figure 1C and D, the hydrophobic core of Kir1.1 contains two aromatic (F194 and Y314) and four hydrophobic (A198, L209, V295 and V319) residues. Homologous amino acids are either identical or similar across the Kir channel family (Fig. 1E), indicating they play essential roles in channel structure and/or function. Notably, mutation of A198 to threonine (A198T) and Y314 to cysteine (Y314C) gives rise to Bartter syndrome.[36]

IgLD core mutations destabilize the Kir channel cytoplasmic domain.

The immunoglobulin-like β-sandwich fold is one of the most common structural domains in the SCOP database, comprising 27 superfamilies and 55 families of proteins. The thermodynamic and mechanical properties as well as the folding pathways for some β-sandwich domains have been examined in detail.[34,37–39] Mutations within the hydrophobic core are generally destabilizing and cause severe protein misfolding in some cases. However, even structurally similar β-sandwich domains within the same superfamily can exhibit variable responses to core mutations.[40] As noted above, the Kir1.1 channel core contains two residues (A198 and Y314) that are mutated in ABS, suggesting they may lead to core instability and misfolding. To our knowledge, the biophysical properties of an E-set IgLD have not yet been examined. We therefore performed computational alanine-scanning mutagenesis to evaluate the contribution of individual residues to the thermodynamic stability of the Kir channel cytoplasmic domain.

Computational mutagenesis was performed on the Kir2.1L cytoplasmic domain X-ray structure (PDB code 1U4F)[14] using the ROSETTA program.[41] ROSETTA models each side chain as a conformational rotamer on a fixed polypeptide backbone. Following mutation, all residues with at least one side-chain atom within five Å of the mutated amino acid are repacked using a Monte Carlo simulated annealing approach. The calculated change in total free energy ($\Delta\Delta G_{calc}$) is derived from a sum of terms accounting for atomic packing interactions, solvation energetics, hydrogen-bonding and electrostatic potentials, rotamer probabilities, and an estimate of unfolded reference state energy.[41]

Alanine mutagenesis-induced changes in $\Delta\Delta G_{calc}$ were calculated for all 788 residues of the tetrameric structure and rank ordered. The average minimum, maximum and median values of $\Delta\Delta G_{calc}$ were −1.4 kcal mol^{-1}, 7.8 kcal mol^{-1} and 1.8 kcal mol^{-1}, respectively. Negative values indicate a stabilizing effect of the alanine substitution, whereas positive values indicate thermodynamic instability. The larger the positive value, the greater the destabilizing effect of the mutation. As shown in Table 1, core mutations produced large positive changes in $\Delta\Delta G_{calc}$ ranging from 2.5 to 4.3 kcal mol^{-1}. Among the 197 residues of each subunit, core residues ranked at the top ~80–95% of most destabilizing mutations. These results are consistent with the notion that that the IgLD core is essential for stabilizing the Kir channel cytoplasmic domain.

The IgLD core tyrosine stabilizes the channel through hydrophobic core packing.

As noted earlier, IgLD cores usually contain one or two aromatic amino acids surrounded by smaller hydrophobic side chains. Core aromatic residues tend to be highly conserved. Chothia et al. (1998) reported that of more than 5,000 V-set Ig domains analyzed, 99% of those have a tyrosine residue in their core.[35] The E-set IgLD core of Kir channels is no exception; the Kir1.1 channel core contains a highly conserved tyrosine residue at position 314 (Fig. 1). Mutation of this tyrosine to cysteine (Y314C) gives rise to loss-of-function channels underlying ABS.[36] In most of IgLD structures studied to date, the core tyrosine hydroxyl group forms a hydrogen bond with the polypeptide backbone of the adjacent loop connecting the two β-sheets. This so-called “tyrosine-corner” motif plays an essential role in stabilizing β-sandwich domains.[34,42,43] We were therefore surprised to find that a tyrosine-corner motif is not present in Kir channels. Instead, the IgLD tyrosine projects across the core to establish a hydrogen bond with the apposing β-sheet. In the Kir1.1 model, the Y314 hydroxyl group forms a hydrogen bond with the backbone carbonyl of serine 195 in the βB-B’ linker located approximately 3 Å away (Fig. 2A). The trans-core hydrogen bond is present in all available mammalian Kir channel crystal structures. We therefore set out to determine if this bond is necessary for Kir1.1 channel stability and function.

Toward this end, we systematically explored how changes in side chain structure (Fig. 2C) affect Kir channel thermodynamic stability using ROSETTA, as described above. All 19 amino acid substitutions were analyzed in silico, the results of which are shown in Figure 2B. All values of $\Delta\Delta G_{calc}$ were positive, indicative of structural instability, and ranged from ~1–8 kcal mol^{-1}. The Y→F substitution, which removes only the hydroxyl group (Fig. 2C) necessary for hydrogen bond formation, was the least destabilizing of the mutations (Fig. 2B), consistent with the notion that trans-core hydrogen bonding plays only a minor role in maintaining channel stability.

Hydrophobic core packing near position 314 appeared to be much more important for stabilizing the channel. Substitution of a tryptophan (W), which retains a bulky hydrophobic side chain but increases its volume by ~18% (Y = 194 $Å^3$, W = 228 $Å^3$) caused a ~5 kcal mol^{-1} calculated change in stability. Similarly, substitution with the aromatic hydrophilic side chain of histidine (H) led to a $\Delta\Delta G_{calc}$ of 4 kcal mol^{-1} (Fig. 2B). Interestingly, the Y→isoleucine (I) mutation led to a calculated change in free energy of only ~2 kcal mol^{-1}, whereas the structurally conservative Y→ leucine (L) substitution was second-most destabilizing ($\Delta\Delta G_{calc}$ ~7 kcal mol^{-1}). These data suggest that even minor changes in side chain packing in the IgLD core can have dramatic effects on the thermodynamic stability of the cytoplasmic domain.

Structurally conservative mutations of tyrosine 314 abolish channel function.

Whole-cell patch clamp electrophysiology was used to assess the functional properties of Y314 mutant channels. Figure 3A (left) shows a family of wild-type (WT) current traces recorded from transfected cells bathed in a 50 mM K^+-containing buffer. WT channels exhibited a linear current-voltage (I-V) relationship between −120 mV and 80 mV, reversed near the theoretical K^+ equilibrium potential (−25 mV) and rectified weakly at large positive test potentials. Channel activity was inhibited by 2 mM Ba^{2+} (Fig. 3A, right) and nanomolar

concentrations of tertiapin-Q (TPNQ; Fig. 4), two well known blockers of Kir1.1.[1,44–46] In striking contrast, cells expressing the ABS mutant Y314C produced no Ba^{2+}-inhibitable inward currents, only small-amplitude outward currents (Fig. 3B) also observed in parental cells (data not shown). The mean ± SEM I-V relationships recorded from cells expressing WT (n = 9) and Y314C-Kir1.1 (n = 16) are shown in Figure 3C. Note the prominent rectification of the WT current at test potentials greater than 80 mV (Fig. 3C). This will be discussed further below.

Five additional Y314 mutants (Y314→F, I, H, W, L) spanning the $\Delta\Delta G_{calc}$ distribution (Fig. 2B) were selected for electrophysiological analysis. As shown in Figure 3D, substitution of W (n = 7), H (n = 6), L (n = 8) or I (n = 10) at position 314 led to a complete loss of channel function. The Y314F (n = 13) substitution, however, did not significantly (p = 0.3) inhibit channel activity (Fig. 3D). Taken together, our computational and electrophysiological data indicate (1) that the trans-core hydrogen bond is not essential for Kir1.1 channel function, and (2) hydrophobic core packing near Y314 plays a key role in channel stability and function.

IgLD core instability impairs Kir1.1 channel trafficking.

Thermodynamic instability caused by mutations in β-sandwich structures can lead to protein misfolding and impairment of trafficking through the secretory pathway.[47,48] We therefore postulated that the Y314C mutation, which produced a calculated 6 kcal mol^{-1} decrease in channel stability (Fig. 2B), would impair channel biosynthesis and trafficking to the cell surface. To test this hypothesis, we generated stably transfected HEK-293 cells expressing WT- or Y314C-Kir1.1 under the control of a tetracycline (Tet)-inducible promoter. A Tet-regulatable system was used to avoid cytotoxic effects of constitutive Kir1.1 channel expression.[36,49]

Kir1.1 is glycosylated on asparagine (N) 117 in the ER and undergoes further oligosaccharide processing in the Golgi apparatus to its fully mature glycosylated form. This produces biochemically distinct populations of channels that can be exploited in endoglycosidase assays to follow trafficking through the secretory pathway.[50] Figure 4A shows a representative immunoblot of whole-cell lysates prepared from parental (i.e., non-transfected) or stably transfected cell lines cultured without (−) or with (+) Tet to induce channel expression. In both WT and Y314C cells, Tet induced multiple Kir1.1-immunoreactive bands that were not observed in parental or uninduced cell lysates (Fig. 4A). The channel protein migrated as a minor band of ~45 kDa, a major ~47 kDa band and a higher molecular weight “smear” of bands centered at ~60 kDa. The higher molecular weight bands collapsed into the 45 kDa band when cells were cultured with the N-glycosylation inhibitor tunicamycin (data not shown), indicating they represent differentially glycosylated forms of the channel protein.

We exploited the glycosylation state of Kir1.1 to determine if the Y314C mutation impairs trafficking through the secretory pathway. Endoglycosidase H (Endo H) preferentially cleaves high-mannose oligosaccharides from immature glycoproteins in the ER, but subsequent N-glycan processing in the medial Golgi renders oligosaccharides insensitive to Endo H. Resistance to Endo H is thus a biochemical marker of channels that have undergone

ER-to-Golgi transport. Figure 4B shows a representative experiment in which lysates were treated with Endo H (left) or PNGase F (right), a pan-endoglycosidase that cleaves all N-linked oligosaccharides. In both cell lines, Endo H collapsed the 47 kDa band into the 45 kDa band, but had no effect on high molecular weight smear. In contrast, PNGase F abolished both high molecular weight species. Taken together, the differential sensitivity of the channel to EndoH and PNGase F indicate that the 47 kDa and 60 kDa bands are the ER- and Golgi-processed forms of the channel, respectively. Quantitative densitometry (Fig. 4C) revealed that the abundance of the Y314C mature glycosylated species was only 36 ± 7% (n = 7) of that of the WT channel.

Having established biochemical “fingerprints” for the different glycoforms of Kir1.1, we returned to the series of Y314 mutants to determine if there is a relationship between computationally derived values of channel stability (Fig. 2B) and channel expression and/or trafficking. Western blot analysis was performed on HEK-293 cells transiently transfected with WT, Y314F, Y314I or Y314L Kir1.1 (Fig. 4). Densitometry was used to quantitate total channel expression (i.e., unglycosylated + core glycosylated + mature glycosylated). The results from 4–5 independent experiments are summarized in Figure 4E. Expression of the fully functional Y314F mutant (Fig. 3D), which lost only a ~1 kcal mol^{-1} in calculated free energy, was approximately 40% higher than that of the WT channel. In contrast, expression of the non-functional Y314I mutant ($\Delta\Delta G_{calc}$ ~2 kcal mol^{-1}) was reduced by approximately 10%. Y314L was also assessed because leucine is structurally very similar to isoleucine (Fig. 2C) but was predicted to be more destabilizing ($\Delta\Delta G_{calc}$ ~6 kcal mol^{-1}) than Y314I. In agreement with our stability calculations (Fig. 2B), expression of the Y314L mutant was reduced by approximately half compared to the WT channel (Fig. 4).

The dramatic reduction in channel mature glycosylation caused by mutations of Y314 suggested that only a fraction of mutant channels are competent for ER export and transport to the cell surface. We tested this hypothesis explicitly in cell surface biotinylation experiments. To facilitate immunodetection of the channel, Tet-inducible HEK-293 cell lines expressing antigenic epitope-tagged WT- or Y314C-Kir1.1 were generated. Addition of the C-terminal V5-tag had no effect on the functional properties (not shown) or glycosylation pattern of the WT or mutant channel (Fig. 5A, middle). Cell surface glycoproteins were biotinylated and immunoprecipitated overnight using streptavidin-conjugated beads. The eluted proteins were separated electrophoretically, transferred to nitrocellulose membrane and blotted using either V5- or Kir1.1-specific antiserum. As shown in the top panel of Figure 5A and summarized in Figure 5B, the abundance of biotinylated Y314-Kir1.1 expressed at the cell surface was reduced by approximately 70% (n = 3) compared to that of the WT channel. Taken together, our data strongly suggest that thermodynamic instability in the IgLD core impairs Kir1.1 K^+ channel biogenesis and trafficking to the cell surface.

Y314C mutant channels expressed at the cell surface are non-functional.

Our biochemical studies demonstrated that a minor fraction of Y314C mutants are processed in the Golgi apparatus (Fig. 4) and reach the cell surface (Fig. 5A and B). To corroborate our patch clamp experiments on transiently transfected cells and determine if cell surface-resident Y314C channels are functional in stably transfected cells, we quantitated WT and

Y314C channel activity using a novel cell-based fluorescence assay. The assay measures Tl^+ flux through Kir1.1 with the fluorescent dye FluoZin-2 (see Methods for details). The main advantage of the assay for the present study is that it enables quantitation of channel activity in thousands of cells simultaneously, providing a robust measure of channel function in large cell populations. Figure 5C shows representative fluorescence traces recorded from WT (left) or Y314C (left) cells incubated without (green) or with (red) the Kir1.1 channel blocker TPNQ. In WT cells (Fig. 5C, left), extracellular Tl^+ addition (arrowhead) evoked an abrupt increase in FluoZin-2 fluorescence (green trace) that was significantly ($p < 0.001$) inhibited by TPNQ (Fig. 5D). In contrast, no TPNQ-inhibitable Tl^+ flux was observed in Y314C cells (Fig. 5C and D). Thus, the Y314C mutant is non-functional in stably transfected cells.

IgLD core disruption by the A198T mutation mimics the effects of Y314C.

Our computational (Fig. 2B) and electrophysiological (Fig. 3D) studies indicated that core packing near Y314 is a major determinant of Kir1.1 channel stability. Molecular modeling suggested that the side chain of A198, which is located on β_1 directly across from Y314, comes to within 4 Å of Y314 (Fig. 1D). We therefore postulated that if side chain packing near Y314 is essential for core stability and if A198 and Y314 are located near one another as our model suggests, then a disruptive mutation of A198 should recapitulate the effects of a Y314 mutation. We selected for study the ABS mutation A198T, which introduces a hydrophilic side chain into the core near Y314. Consistent with our hypothesis, A198T-Kir1.1 was non-functional in transiently (Fig. 6A) and stably transfected (Fig. 6B) cells and, like Y314C-Kir1.1, Golgi processing A198T-Kir1.1 was reduced by approximately 80% (Fig. 6C and D). Taken together, these data support our conclusion that mutations disrupting hydrophobic core packing between β_1 and β_2 lead to impaired channel stability, trafficking and function.

IgLD core mutations disrupt gating at the helix-bundle crossing.

Despite the fact that some core mutants reach the cell surface (Fig. 5), we were unable to detect activity from these channels in patch clamp experiments (Fig. 3) or Tl^+ flux assays (Figs. 5 and 6). This suggested that core mutants may be electrically silent due to defects in channel gating. As noted earlier, several ABS mutations have been shown to shift the apparent acid dissociation constant (pKa) in the alkaline direction, causing the channels to be electrically silent at physiological pH_i. The molecular mechanisms coupling pH_i to Kir1.1 channel gating are not fully understood, but clearly involve lysine 80 (K80) of the so-called “RKR triad”.[26] Lysine 80 is located near the cytoplasmic end of the membrane-spanning pore in a structure termed the helix-bundle crossing. Mutation of K80 to methionine (K80M) dramatically shifts the pKa of Kir1.1 in the acid direction, leading to constitutive channel activity over a broader range of pH_i values.[21,26,51] Importantly, the K80M mutation has been shown to rescue the function of some gating mutants by shifting the pKa back to the physiological range.[23,28] If cell surface A198T and Y314C channels are electrically silent due to closure of the pH_i gate, we postulated that a secondary K80M mutation would rescue channel activity.

Whole-cell currents were recorded from HEK-293 cells expressing single mutants A198T or Y314C, double mutants A198T/K80M or Y314C/K80M, or the K80M background mutant as a control. The results are summarized in Figure 7. Consistent with our earlier observations (Fig. 3C), Kir1.1-mediated macroscopic channel activity was not observed in cells expressing A198T or Y314C (Fig. 7B and C). The mean ± SEM current amplitude recorded at −120 mV from A198T- and Y314C-expressing cells was −5.1 ± 1.2 pA/pF (n = 6) and −0.4 ± 0.2 pA/pF (n = 6), respectively (Fig. 7B). About half of the cells expressing A198T/K80M (5 out of 12 cells) or Y314C/K80M (nine out of 17 cells) generated less than −10 pA/pF of Ba^{2+}-inhibitable current. In the remaining cells, however, the K80M-double mutants produced clear Kir1.1-mediated channel activity (Fig. 7C). Representative current traces recorded between −120 mV and 120 mV from cells expressing K80M (left), A198T/K80M (middle) and Y314C/K80M (right) are shown in Figure 7A. The mean ± SEM current amplitude for A198T/K80M (n = 12) and Y314C/K80M (n = 17) cells was −52.5 ± 15.3 and −58.1 ± 26.1, respectively. These mutant current values are significantly different from those recorded from K80M-expressing cells (mean ± SEM = −264.8 ± 44.9; n = 28; Fig 7B). Furthermore, this approximately 80% reduction in mutant channel activity is in good agreement with our biochemical data indicating a ~70–80% reduction in mutant channel trafficking (Figs. 4C, 5B and 6C and D). Taken together, these data strongly support the conclusion that core mutations impair anterograde trafficking and gating at the helix-bundle crossing.

IgLD core mutations abolish Kir1.1 current rectification.

During the course of our studies, we noted that K80M-rescued core mutants failed to rectify at positive test pulses. This is clearly observed by plotting I-V relationships (Fig. 7D) from the representative current traces shown in Figure 7A. Like the WT channel, K80M (black filled circles) exhibited prominent rectification at voltages above 80 mV (Fig. 7D). However, neither A198T/K80M (open circles) nor Y314C/K80M (grey filled circles) mutants showed rectification at potential up to 120 mV. We quantitated this effect by calculating a “rectification coefficient” (R.C.) for WT, K80M, A198T/K80M and Y314C/K80M channels, the results of which are shown in Figure 7E. WT-Kir1.1 exhibited the strongest rectification with a mean ± SEM R.C. of 2.4 ± 0.1 (n = 27). K80M also exhibited pronounced rectification (R.C. = 1.9 ± 0.1, n = 14), albeit to a significantly ($p < 0.02$) lesser degree than WT channels (Fig. 7E). The R.C. for A198T/K80M (1.1 ± 0.1; n = 6) and Y314C/K80M (1.1 ± 0.1; n = 5) were significantly ($p < 0.01$) smaller than that of K80M, but were not different ($p > 0.05$) from a value of 1.0, indicating that the core mutants have effectively lost their rectification properties. Non-rectifying currents were not caused by activation of a leak pathway, because the mutant channel currents reversed near the calculated K^+ equilibrium potential (e.g., Fig. 7D) and were inhibited by Ba^{2+} (Fig. 7B).

Discussion

Since the discovery that heritable mutations in Kir1.1 cause ABS,[52] surprisingly little progress has been made toward elucidating the molecular and cellular mechanisms underlying channel dysfunction in this life-threatening disease. The recent determination of atomic structures for bacterial and mammalian Kir channel proteins[9,10,14,24,29,30] creates

unprecedented opportunities for applying novel structural and computational methods to define Kir channel structure-function relationships underlying ABS. In the present work, we exploited molecular modeling and computational mutagenesis, as well as conventional biochemical and electrophysiological approaches, to examine a heretofore uncharacterized E-set IgLD in the C-terminus of Kir1.1. We show that thermodynamically debilitating mutations within the IgLD core are associated with striking defects in channel processing, trafficking, gating and stability. Our study sheds new light on the pathogenesis of ABS and provides a novel structural framework for understanding Kir channel function.

We confirmed and extended the findings of Peters et al.,[36] who surveyed function of 20 ABS mutants heterologously expressed in *Xenopus* oocytes and immunofluorescence localization in oocytes and HEK-293 cells. They reported that more than half of the loss-of-function mutants, including A198T and Y314C, are not expressed at the plasma membrane.[36] The subcellular localization of ABS mutants was not defined. Here we showed that the steady-state abundance of Golgi-processed Kir1.1 is dramatically reduced by IgLD core mutations, suggesting that core mutations impair subunit folding and trafficking out of the ER. Indeed, work on other β-sandwich domains supports a role for core mutation-induced subunit misfolding.[34,37–39,53] Every Ig domain family member studied to date folds by a nucleation-condensation mechanism whereby a folding nucleus comprised of linearly distant hydrophobic residues coalesce to form a common structural core; early core packing during folding ensures formation of the correct native-state topology. The core tyrosine residue present in most β-sandwich domains is critical for protein stability. Mutation of core tyrosine residues can slow protein folding, destabilize the native-state structure or, in extreme cases, prevent folding altogether. Although the Y314C mutation is highly destabilizing, it does not prevent subunit folding. Oligomeric proteins such as Kir channels must be assembled in the ER before they can pass ER quality control and be exported to the Golgi apparatus for further biosynthetic processing. We demonstrated that a fraction of Y314C-Kir1.1 is processed in the Golgi and incorporated into the cell membrane. Thus, Y314C mutants fold well enough to support channel assembly and trafficking to the cell surface. Our biotinylation studies revealed for the first time that all three glycoforms of Kir1.1 channel subunits (i.e., unglycosylated, immature glycosylated and mature glycosylated) could be immunoprecipitated from the cell surface of mammalian cells. This indicates that not all subunits of the tetrameric channel undergo mature processing in the Golgi apparatus, at least under the expression conditions employed.

The core mutant Y314L showed no evidence of biosynthetic processing beyond the ER. Furthermore, the abundance of Y314L was dramatically reduced compared to that of WT or other mutant channels, consistent with the notion that the Y→L mutation leads to subunit misfolding, ER retention and ER-associated degradation. Studies are underway to define Kir1.1 channel degradation mechanisms in mammalian cells. Trafficking-defective core mutant channels (e.g., Y314C/L) should be useful tools for defining these pathways.

We showed that the K80M substitution rescues function of channels harboring either A198T or Y314C mutations. At present, we can only speculate about possible mechanisms linking mutations in the cytoplasmic domain to gating at the helix-bundle crossing. However, it should be noted that the peripheral loops extending from the IgLD include the “G-loop” and

"CD-loop" (Fig. 1B), both of which participate in channel gating.[14,18,30] Future studies will address whether these loops could mediate communication between the IgLD and helix-bundle gate.

The discovery of numerous disease-causing mutations in the IgLD of Kir1.1 (A214V, S219R, L220F, A306T, R311W/Q, S313C, Y314C, V315G, L320P) and Kir2.1 (N216H, L217P, R218W/Q, G300D/V, V302M, E303K, R312C, Δ314–315) underscores the importance of this domain for Kir channel function. We ultimately wish to know how disease-causing mutations alter the atomic structure and hence function of Kir channels. X-ray crystallography is beginning to shed light on the matter,[30] but ion channel crystallography is still in its infancy and not yet widely used. An alternative approach is the use of pharmacological or cysteine reactive compounds to probe the structure of the channel in electrophysiological experiments. Progress on this front has been limited in part by the fact that many ABS and Andersen syndrome mutants are non-functional and are thus not amenable to electrophysiological analysis. The ability to record channel activity in "loss-of-function" Kir1.1 channel mutants carrying the second-site K80M substitution creates opportunities for defining structural changes in ABS mutant channels using electrophysiology. For example, we found that K80M-rescued core mutants fail to exhibit Mg^{2+}-dependent rectification. As noted earlier, the strength of Kir channel rectification is determined in part by the presence of charged residues lining the conduction pathway that influence the binding of blocking cations in the pore. The loss of rectification in these mutants strongly suggests that stable Mg^{2+} binding is disrupted by core mutations. Because the side chains of A198 and Y314 are buried within the core, it is very unlikely that these residues mediate Mg^{2+} binding directly. Rather, the most parsimonious explanation is that core mutations alter the structure of the pore and indirectly destabilize interactions of Mg^{2+} with pore-lining residues. Electrophysiological studies using Mg^{2+} or other intracellular pore blockers[54,55] may help determine if and how IgLD core mutations alter pore structure.

We postulate that the IgLD places critical steric constraints on the range of possible gating conformations in Kir channels, as follows. The cytoplasmic domain contains seven major β-strands, all of which are part of either β_1 or β_2 (Fig. 1). The sheets are packed face-to-face with an intervening hydrophobic core that stabilizes their association. As a result, and due to the inherent mechanical properties of β-pleated sheets, all seven β-strands will tend to behave as a single rigid body. In the simplest interpretation of the model, the 28 β-sheets comprising about half of the cytoplasmic domain are reduced to four rigid Ig domains. In support of this model, recent X-ray studies of a Kir channel chimera provided structural evidence for rigid-body motions within the cytoplasmic domain.[10] Detailed studies of the IgLD should deepen our understanding of cytoplasmic domain gating mechanisms and motions in Kir channels.

Materials and Methods

Reagents and chemicals.

Parental Tetracycline-Regulated Expression (T-REx) Human Embryonic Kidney (HEK)-293 cells, Dulbecco's Modified Eagle Medium (DMEM) containing 25 mM D-glucose and 2 mM L-glutamine, bovine serum albumin (BSA), anti-V5 antiserum and the acetoxymethyl

(AM) ester form of FluoZin-2 were purchased from Invitrogen (Carlsbad, CA). Tertiapin Q (TPNQ), Protease Inhibitor Cocktail, Triton X-100, TWEEN-20, and salts of the highest purity available were purchased from Sigma-Aldrich (St. Louis, MO). Fetal bovine serum (FBS) was from Atlanta Biologicals (Lawrenceville, GA). Thallium (I) sulfate was from Alfa Aesar (Ward Hill, MA). Rabbit polyclonal antiserum raised against the carboxyl terminus of rat Kir1.1 (amino acids 342–391) was purchased from Alomone Labs (Jerusalem, Israel). Rabbit β-actin antiserum was from Santa Cruz, (Santa Cruz, CA). HRP-conjugated goat anti-rabbit secondary antiserum was from Jackson ImmunoResearch Laboratories (West Grove, PA). SuperSignal West Pico chemiluminescent reagent and BCA protein quantitation kit were purchased from Pierce (Rockford, IL).

Tetracycline HCl (Sigma) and Blasticidin S HCl (Invitrogen) were prepared as 1 mg/ml and 5 mg/ml stock solutions, respectively, in molecular-grade water, sterile filtered and stored at −20°C in single-use aliquots. Hygromycin B (Invitrogen), provided as a 50 mg/ml stock solution in PBS was stored at 4°C until time of use.

Molecular biology.

The rat Kir1.1a channel cDNA in pcDNA3.1 was generously provided by Dr. Chun Jiang (Georgia State University) with permission from Dr. Steven Hebert (Yale University). Site-directed mutagenesis was performed using the QuickChange II kit (Stratagene, La Jolla, CA). Kir1.1 was sub-cloned into pcDNA5/TO (Invitrogen) using KpnI and NotI restriction sites. pcDNA3.1-Kir1.1-V5-His was created by TOPO cloning a Kir1.1 cDNA PCR fragment lacking a stop codon into pcDNA3.1-V5-His-TOPO (Invitrogen) in frame with the 3’ epitopes. A Kir1.1-V5-His PCR fragment containing a Kozak sequence (GCCGCC) and KpnI and BamHI sites was cloned into pcDNA5/TO. All PCR products were sequenced to ensure fidelity.

Generation of tetracycline-inducible cell lines.

Parental T-REx-HEK-293 cells stably transfected with the pcDNA6/TR vector, which drives high-level expression of the tetracycline (Tet) repressor (TR), were cultured at 37°C in a 5% CO_2 incubator in DMEM supplemented with 10% FBS, 0.5% Pen-Strep and 5 μg/ml blasticidin (b-DMEM). The day before transfection, 6×10^6 cells were plated in 75 cm^2 flasks and grown to approximately 60% confluence overnight. The cells were subsequently transfected with 25 μg of pcDNA5/TO-Kir1.1 plasmid DNA using Lipofectamine 2000 (Invitrogen) according the manufacturer’s instructions. This vector contains a cytomegalovirus (CMV) promoter harboring two TR binding sites. In the absence of Tet, the TR proteins occupy their binding sites in the CMV promoter and block Kir1.1 transcription. TR proteins are displaced from the promoter in the presence of Tet, thereby enabling Tet-inducible channel expression. The day after transfection, the cell culture media was replaced with b-DMEM containing 250 μg/ml hygromycin (bh-DMEM) to select for doubly transfected cells. Stable polyclonal cell lines were expanded for approximately 3 weeks and cryopreserved. Cell lines were used for no more than 20 passages. In all experiments, cells were cultured overnight with 1 μg/ml Tet to induce channel expression.

Cell lysis and immunoblot analysis.

Cells were washed three times with ice-cold phosphate-buffered saline (PBS) and solubilized in ice-cold buffer containing 150 mM NaCl, 100 mM NaF, 50 mM tris-HCl (pH 8.0), 35 mM sodium deoxycholate, 5 mM EDTA, 1% Triton X-100, 0.1% SDS and 1X Protease Inhibitor Cocktail. Cell lysates were scraped into Eppendorf tubes, sonicated, rotated end-over-end for 30 min at 4°C and then centrifuged for 10 min to pellet insoluble material. The protein concentration of cleared lysates was quantitated using BCA reagent. Lysates were either used immediately or frozen as single-use aliquots at −80°C for subsequent immunoblot analysis.

Lysate protein was separated electrophoretically using 10% Bis-Tris NuPAGE gels (Invitrogen) and transferred to 0.45 μm pore nitrocellulose membranes (BioRad, Hercules, CA). Membranes were blocked overnight at 4°C in Tris-buffered saline (25 mM Tris, 1.3 mM KCl and 137 mM NaCl) containing 0.1% TWEEN-20 (TBST) and 5% non-fat milk, probed at room temperature for 4 h in Kir1.1 antiserum (1:500 in milk-TBST) and then incubated at room temperature for 1 h in HRP-conjugated secondary antiserum (1:40,000 in milk-TBST). Protein bands were visualized on film using enhanced chemiluminescence detection methods. Antibodies were stripped from membranes in buffer containing 100 mM 2-mercaptoethanol, 62.5 mM Tris-HCl (pH 6.7) and 2% SDS (50°C for 30 min) and re-probed with β-actin antiserum to ensure equal protein loading.

Endoglycosidase digestion.

The glycosylation state of Kir1.1 was assessed by immunoblot analysis of cell lysates treated with PNGase F or Endo H (New England Biolabs, Ipswich, MA), as follows. Fifteen μg of lysate protein in a 10 μl reaction volume was denatured in glycoprotein denaturing buffer (NEB) at room temperature for 10 min. The denatured protein was treated for 1 h at room temperature with 1,000 U (PNGase F) or 2,000 U (Endo H) of enzyme in a 20 μl reaction containing 1X enzyme buffer. Lysates treated without enzyme served as the control. Immunoblot analysis was performed as described above.

Cell surface biotinylation.

Tet-induced cells (1×10^5 cells/cm^2) stably transfected with V5-His-tagged WT or Y314C-Kir1.1 were washed three times in ice-cold PBS containing 1 mM $MgCl_2$ and 0.1 mM $CaCl_2$ (buffer A). All of the following steps were performed on ice or at 4°C using ice-cold solutions. Membrane proteins were oxidized for 30 min with 10 mM sodium meta-periodate freshly dissolved in buffer A, washed 3 times in buffer A and rinsed with 100 mM sodium acetate (pH 5.5) containing 1 mM $MgCl_2$ and 0.1 mM $CaCl_2$ (buffer B). The cells were subsequently incubated with 2 mM biotin long-chain hydrazide (Pierce) dissolved in buffer B and rocked gently for 30 min. Buffer B lacking biotin was added to cells as a control. Cells were washed once with quenching buffer containing 50 mM Tris-HCl in buffer A (pH 7.4), washed twice in buffer A, washed twice in divalent-free PBS, and lysed as described above.

Biotinylated proteins were immunoprecipitated from whole-cell lysates (40 μg in 900 μl of cell lysis buffer) overnight at 4°C with end-over-end rotation using 100 μl of a 50% slurry of

washed streptavidin agarose resin (Pierce). The next day, the resin was washed extensively, pelleted by brief centrifugation and dried by aspirating the supernatant with a gel-loading tip. Immunoprecipitated proteins were eluted at 85°C for 2 min in 1X LDS buffer (Invitrogen) and 1X reducing agent (Invitrogen) containing 50 mM DTT. Eluted proteins were separated electrophoretically, transferred to nitrocellulose membrane, blocked for 1 h in milk-TBST and probed overnight at 4°C with V5 antiserum (diluted 1:3,000). Protein bands were visualized as described above.

Thallium flux assays.

A modification of the thallium (Tl^+) flux assay reported by Weaver et al. (2003) was used to assess channel function in stable cell lines.[56] Cells (30,000/well) were plated in a clear-bottomed, 384-well plate and cultured overnight in serum-free media containing Tet to induce channel expression. The cells were loaded with the AM ester of FluoZin-2 for 45 minutes and washed with Assay Buffer (Hank's Buffered Salt Solution supplemented with 20 mM HEPES, pH 7.3). The cell plate was loaded into a Hamamatsu FDSS6000 kinetic imaging plate reader for measurement of Tl^+-induced increase in FluoZin-2 fluorescence. The FDSS6000 is equipped with an integrated liquid handling system and a CCD camera that records fluorescence emission from all 384 wells simultaneously. Upon addition of Tl^+ stimulus buffer (125 mM sodium gluconate, 12 mM thallium sulfate, 1 mM magnesium sulfate, 1.8 mM calcium gluconate, 5 mM glucose, 10 mM HEPES, pH 7.3), images were collected at 1 Hz for 2 min. The slope of the Tl^+-induced FluoZin-2 fluorescence increase recorded between 7 and 12 sec following Tl^+ addition is used as a measure of Tl^+ flux and hence channel activity.

Transient transfection and patch clamp electrophysiology.

HEK-293 cells (CRL-1573; ATCC) were cultured in Eagle's minimal essential medium (GIBCO BRL) containing 10% FBS, nonessential amino acids, sodium pyruvate, 50 U/ml penicillin and 50 μg/ml streptomycin. Cells were transfected with 500 ng of channel expression vector and 500 ng of pcDNA3.1-EGFP (transfection marker) using Lipofectamine 2000 as directed by the manufacturer. Patch clamp experiments were performed 24 h post-transfection. The day of experiments, transfected cells were rinsed with divalent-free buffer (145 mM NaCl, 5 mM KCl, 4 mM $NaHCO_3$, 0.3 mM Na_2HP0_4, 0.3 mM KH_2PO_4, 5.6 mM D-glucose, pH 7.4, 290 mOsm), dissociated by brief exposure to 0.25% Trypsin containing 1 mM EDTA, plated on poly-L-lysine-coated round glass coverslips and allowed to recover at 37°C in a 5% CO_2 incubator for at least 1 h before initiating electrophysiological experiments. Plated coverslips were transferred to a small-volume perfusion chamber (Warner Instruments, Hamden, CT) and mounted on the stage of a Nikon Eclipse TE2000-U inverted microscope.

Patch electrodes were pulled from silanized 1.5-mm outer diameter borosilicate microhematocrit tubes using a Narishige PP-830 two-stage puller. Electrode resistance ranged from 2.5 to 3.5 MΩ when filled with the following intracellular solution (in mM): 135 KCl, 2 $MgCl_2$, 1 EGTA, 10 HEPES free acid, 2 Na_2ATP (Roche, Indianapolis, IN), pH 7.3, 275 mOsm. The standard bath solution contained (in mM): 90 NaCl, 50 KCl, 2 $CaCl_2$, 1 $MgCl_2$, 5 glucose, 10 HEPES free acid, pH 7.4, 290 mOsm.

Whole-cell currents were recorded under voltage-clamp conditions using an Axopatch 200B amplifier (Molecular Devices, Sunnyvale, CA). Electrophysiological data was collected at 5 kHz and filtered at 1 kHz. Electrical connections to the amplifier were made using Ag/AgCl wires and 3 M KCl/agar bridges. Current-voltage (I-V) relationships were generated by stepping the cell voltage between −120 mV and 120 mV in 20 mV increments for 500 msec from a −75 mV holding potential. Test pulses were delivered every 5 sec and returned to the holding potential between steps. Mean current amplitude recorded over the last 10 msec of each test pulse was normalized to cell capacitance and plotted as a function of test voltage to generate current-voltage relationships.

Molecular modeling.

A model was constructed for the Kir1.1a channel using MODELLER.[57] Initially, a multiple sequence alignment was performed on Kir1.1a, Kir2.1, Kir3.1 and a chimeric protein composed of the cytoplasmic domain of Kir3.1 and the transmembrane domain from KirBac1.3,[10] using the BCL_align sequence alignment package.[58] Using this alignment, a preliminary homology model for residues 39–362 of the tetrameric channel was generated based on the crystal structure of the chimera (PDB code 2QKS). Twenty models were constructed using MODELLER 9v1 in the automodel mode, and the lowest energy structure was then refined using 500 steps of energy minimization with the Sander molecular dynamics program from AMBER 7.[59] Molecular graphics images were generated for publication using the UCSF Chimera package from the Computer Graphics Laboratory, University of California, San Francisco (supported by NIH P41 RR-01081).[60]

Computational mutagenesis.

Computational alanine-scanning mutagenesis of the cytoplasmic domain of Kir2.1 was performed using ROSETTA.[41] Briefly, the crystal structure of the cytoplasmic domain of mouse Kir2.1L (PDB code 1U4F) was subjected to an exhaustive alanine scan using the interface mode of ROSETTA to iteratively replace each residue in the protein with alanine and then calculate the change in total energy after repacking and minimization. The side-chains were modeled as rotamers on a fixed backbone template, and optimization of all residues within five Angstroms (Å) of the site of mutation was performed using a Monte Carlo simulated annealing approach.[61] Mutants were sorted by change in free energy to identify the positions displaying the most destabilizing effect. In addition, position 315 of Kir2.1, which is equivalent to Y314 of Kir1.1, was further evaluated by substitution of the tyrosine to all 19 other amino acids in the context of the tetramer.

Statistics.

Data are presented as means ± the standard error of the mean (SEM). Statistical significance was determined with Student's two-tailed t-test for paired or unpaired means. p values of < 0.05 were taken to indicate statistical significance.

Acknowledgements

We wish to thank Dr. Eric Dawson for helpful discussions during the early stages of the work and Dr. David Weaver for help developing the Tl^+ flux assay. Jerod S. Denton is supported by a Beginning Grant-in-Aid (0865106E) from the American Heart Association Southeast Affiliate and faculty development funds. Jens Meiler is supported by

grant R01-GM080403 from the National Institute of General Medical Sciences. Daniel Addison was supported by NIH training grant HL076133-04.

References

1. Ho K, Nichols CG, Lederer WJ, Lytton J, Vassilev PM, Kanazirska MV, et al. Cloning and expression of an inwardly rectifying ATP-regulated potassium channel. Nature 1993; 362:31–8. [PubMed: 7680431]
2. Zhou H, Tate SS, Palmer LG. Primary structure and functional properties of an epithelial K channel. Am J Physiol 1994; 266:809–24.
3. Kubo Y, Baldwin TJ, Jan YN, Jan LY. Primary structure and functional expression of a mouse inward rectifier potassium channel. Nature 1993; 362:127–33. [PubMed: 7680768]
4. Kubo Y, Reuveny E, Slesinger PA, Jan YN, Jan LY. Primary structure and functional expression of a rat G-protein-coupled muscarinic potassium channel. Nature 1993; 364:802–6. [PubMed: 8355805]
5. Hebert SC, Desir G, Giebisch G, Wang W. Molecular diversity and regulation of renal potassium channels. Physiol Rev 2005; 85:319–71. [PubMed: 15618483]
6. Wang WH. Regulation of ROMK (Kir1.1) channels: new mechanisms and aspects. Am J Physiol Renal Physiol 2006; 290:14–9.
7. Peters M, Jeck N, Reinalter S, Leonhardt A, Tonshoff B, Klaus GG, et al. Clinical presentation of genetically defined patients with hypokalemic salt-losing tubulopathies. Am J Med 2002; 112:183–90. [PubMed: 11893344]
8. Bartter FC, Pronove P, Gill JR Jr, Maccardle RC. Hyperplasia of the juxtaglomerular complex with hyperaldosteronism and hypokalemic alkalosis. A new syndrome. Am J Med 1962; 33:811–28. [PubMed: 13969763]
9. Kuo A, Gulbis JM, Antcliff JF, Rahman T, Lowe ED, Zimmer J, et al. Crystal structure of the potassium channel KirBac1.1 in the closed state. Science 2003; 300:1922–6. [PubMed: 12738871]
10. Nishida M, Cadene M, Chait BT, MacKinnon R. Crystal structure of a Kir3.1-prokaryotic Kir channel chimera. EMBO J 2007; 26:4005–15. [PubMed: 17703190]
11. Lu Z, MacKinnon R. Electrostatic tuning of Mg^{2+} affinity in an inward-rectifier K^+ channel. Nature 1994; 371:243–6. [PubMed: 7915826]
12. Wible BA, Taglialatela M, Ficker E, Brown AM. Gating of inwardly rectifying K^+ channels localized to a single negatively charged residue. Nature 1994; 371:246–9. [PubMed: 8078584]
13. Nichols CG, Ho K, Hebert S. Mg^{2+}-dependent inward rectification of ROMK1 potassium channels expressed in *Xenopus* oocytes. J Physiol 1994; 476:399–409. [PubMed: 8057249]
14. Pegan S, Arrabit C, Zhou W, Kwiatkowski W, Collins A, Slesinger PA, Choe S. Cytoplasmic domain structures of Kir2.1 and Kir3.1 show sites for modulating gating and rectification. Nat Neurosci 2005; 8:279–87. [PubMed: 15723059]
15. Kurata HT, Cheng WW, Arrabit C, Slesinger PA, Nichols CG. The role of the cytoplasmic pore in inward rectification of Kir2.1 channels. J Gen Physiol 2007; 130:145–55. [PubMed: 17635958]
16. Fujiwara Y, Kubo Y. Functional roles of charged amino acid residues on the wall of the cytoplasmic pore of Kir2.1. J Gen Physiol 2006; 127:401–19. [PubMed: 16533896]
17. Leung YM, Zeng WZ, Liou HH, Solaro CR, Huang CL. Phosphatidylinositol 4,5-bisphosphate and intracellular pH regulate the ROMK1 potassium channel via separate but interrelated mechanisms. J Biol Chem 2000; 275:10182–9. [PubMed: 10744702]
18. Zeng WZ, Liou HH, Krishna UM, Falck JR, Huang CL. Structural determinants and specificities for ROMK1-phosphoinositide interaction. Am J Physiol Renal Physiol 2002; 282:826–34.
19. Huang CL, Feng S, Hilgemann DW. Direct activation of inward rectifier potassium channels by PIP_2 and its stabilization by Gbetagamma. Nature 1998; 391:803–6. [PubMed: 9486652]
20. Tsai TD, Shuck ME, Thompson DP, Bienkowski MJ, Lee KS. Intracellular H^+ inhibits a cloned rat kidney outer medulla K^+ channel expressed in *Xenopus* oocytes. Am J Physiol 1995; 268:1173–8.
21. Fakler B, Schultz JH, Yang J, Schulte U, Brandle U, Zenner HP, et al. Identification of a titratable lysine residue that determines sensitivity of kidney potassium channels (ROMK) to intracellular pH. EMBO J 1996; 15:4093–9. [PubMed: 8861938]

22. Rapedius M, Fowler PW, Shang L, Sansom MS, Tucker SJ, Baukrowitz T. H bonding at the helix-bundle crossing controls gating in Kir potassium channels. Neuron 2007; 55:602–14. [PubMed: 17698013]
23. Rapedius M, Haider S, Browne KF, Shang L, Sansom MS, Baukrowitz T, Tucker SJ. Structural and functional analysis of the putative pH sensor in the Kir1.1 (ROMK) potassium channel. EMBO Rep 2006; 7:611–6. [PubMed: 16641935]
24. Kuo A, Domene C, Johnson LN, Doyle DA, Venien-Bryan C. Two different conformational states of the KirBac3.1 potassium channel revealed by electron crystallography. Structure 2005; 13:1463–72. [PubMed: 16216578]
25. Zhang YY, Sackin H, Palmer LG. Localization of the pH gate in Kir1.1 channels. Biophys J 2006; 91:2901–9. [PubMed: 16891366]
26. Schulte U, Hahn H, Konrad M, Jeck N, Derst C, Wild K, et al. pH gating of ROMK (Kir1.1) channels: control by an Arg-Lys-Arg triad disrupted in antenatal Bartter syndrome. Proc Natl Acad Sci USA 1999; 96:15298–303. [PubMed: 10611379]
27. Flagg TP, Yoo D, Sciortino CM, Tate M, Romero MF, Welling PA. Molecular mechanism of a COOH-terminal gating determinant in the ROMK channel revealed by a Bartter's disease mutation. J Physiol 2002; 544:351–62. [PubMed: 12381810]
28. Leng Q, MacGregor GG, Dong K, Giebisch G, Hebert SC. Subunit-subunit interactions are critical for proton sensitivity of ROMK: evidence in support of an intermolecular gating mechanism. Proc Natl Acad Sci USA 2006; 103:1982–7. [PubMed: 16446432]
29. Nishida M, MacKinnon R. Structural basis of inward rectification: cytoplasmic pore of the G protein-gated inward rectifier GIRK1 at 1.8 A resolution. Cell 2002; 111:957–65. [PubMed: 12507423]
30. Pegan S, Arrabit C, Slesinger PA, Choe S. Andersen's syndrome mutation effects on the structure and assembly of the cytoplasmic domains of Kir2.1. Biochemistry 2006; 45:8599–606. [PubMed: 16834334]
31. Bujnicki JM, Elofsson A, Fischer D, Rychlewski L. Structure prediction meta server. Bioinformatics 2001; 17:750–1. [PubMed: 11524381]
32. Murzin AG, Brenner SE, Hubbard T, Chothia C. SCOP: a structural classification of proteins database for the investigation of sequences and structures. J Mol Biol 1995; 247:536–40. [PubMed: 7723011]
33. Chothia C, Janin J. Relative orientation of close-packed beta-pleated sheets in proteins. Proc Natl Acad Sci USA 1981; 78:4146–50. [PubMed: 16593054]
34. Hamill SJ, Cota E, Chothia C, Clarke J. Conservation of folding and stability within a protein family: the tyrosine corner as an evolutionary cul-de-sac. J Mol Biol 2000; 295:641–9. [PubMed: 10623553]
35. Chothia C, Gelfand I, Kister A. Structural determinants in the sequences of immunoglobulin variable domain. J Mol Biol 1998; 278:457–79. [PubMed: 9571064]
36. Peters M, Ermert S, Jeck N, Derst C, Pechmann U, Weber S, et al. Classification and rescue of ROMK mutations underlying hyperprostaglandin E syndrome/antenatal Bartter syndrome. Kidney Int 2003; 64:923–32. [PubMed: 12911542]
37. Cota E, Steward A, Fowler SB, Clarke J. The folding nucleus of a fibronectin type III domain is composed of core residues of the immunoglobulin-like fold. J Mol Biol 2001; 305:1185–94. [PubMed: 11162123]
38. Borgia A, Williams PM, Clarke J. Single-molecule studies of protein folding. Annu Rev Biochem 2008; 77:101–25. [PubMed: 18412537]
39. Brockwell DJ, Paci E, Zinober RC, Beddard GS, Olmsted PD, Smith DA, et al. Pulling geometry defines the mechanical resistance of a beta-sheet protein. Nat Struct Biol 2003; 10:731–7. [PubMed: 12923573]
40. Cota E, Hamill SJ, Fowler SB, Clarke J. Two proteins with the same structure respond very differently to mutation: the role of plasticity in protein stability. J Mol Biol 2000; 302:713–25. [PubMed: 10986129]
41. Rohl CA, Strauss CE, Chivian D, Baker D. Modeling structurally variable regions in homologous proteins with rosetta. Proteins 2004; 55:656–77. [PubMed: 15103629]

42. Hemmingsen JM, Gernert KM, Richardson JS, Richardson DC. The tyrosine corner: a feature of most Greek key beta-barrel proteins. Protein Sci 1994; 3:1927–37. [PubMed: 7703839]
43. Nicaise M, Valerio-Lepiniec M, Izadi-Pruneyre N, Adjadj E, Minard P, Desmadril M. Role of the tyrosine corner motif in the stability of neocarzinostatin. Protein Eng 2003; 16:733–8. [PubMed: 14600202]
44. Jin W, Lu Z. A novel high-affinity inhibitor for inward-rectifier K+ channels. Biochemistry 1998; 37:13291–9. [PubMed: 9748337]
45. Zhou H, Chepilko S, Schutt W, Choe H, Palmer LG, Sackin H. Mutations in the pore region of ROMK enhance Ba^{2+} block. Am J Physiol 1996; 271:1949–56.
46. Jin W, Lu Z. Synthesis of a stable form of tertiapin: a high-affinity inhibitor for inward-rectifier K^{+} channels. Biochemistry 1999; 38:14286–93. [PubMed: 10572003]
47. Randles LG, Lappalainen I, Fowler SB, Moore B, Hamill SJ, Clarke J. Using model proteins to quantify the effects of pathogenic mutations in Ig-like proteins. J Biol Chem 2006; 281:24216–26. [PubMed: 16760466]
48. De Angelis E, Watkins A, Schafer M, Brummendorf T, Kenwrick S. Disease-associated mutations in L1 CAM interfere with ligand interactions and cell-surface expression. Hum Mol Genet 2002; 11:1–12. [PubMed: 11772994]
49. Nadeau H, McKinney S, Anderson DJ, Lester HA. ROMK1 (Kir1.1) causes apoptosis and chronic silencing of hippocampal neurons. J Neurophysiol 2000; 84:1062–75. [PubMed: 10938328]
50. Yoo D, Fang L, Mason A, Kim BY, Welling PA. A phosphorylation-dependent export structure in ROMK (Kir 1.1) channel overrides an endoplasmic reticulum localization signal. J Biol Chem 2005; 280:35281–9. [PubMed: 16118216]
51. Choe H, Zhou H, Palmer LG, Sackin H. A conserved cytoplasmic region of ROMK modulates pH sensitivity, conductance and gating. Am J Physiol 1997; 273:516–29.
52. Simon DB, Karet FE, Rodriguez-Soriano J, Hamdan JH, DiPietro A, Trachtman H, et al. Genetic heterogeneity of Bartter's syndrome revealed by mutations in the K+ channel, ROMK. Nat Genet 1996; 14:152–6. [PubMed: 8841184]
53. Forman JR, Qamar S, Paci E, Sandford RN, Clarke J. The remarkable mechanical strength of polycystin-1 supports a direct role in mechanotransduction. J Mol Biol 2005; 349:861–71. [PubMed: 15894330]
54. Rodriguez-Menchaca AA, Navarro-Polanco RA, Ferrer-Villada T, Rupp J, Sachse FB, Tristani-Firouzi M, Sanchez-Chapula JA. The molecular basis of chloroquine block of the inward rectifier Kir2.1 channel. Proc Natl Acad Sci USA 2008; 105:1364–8. [PubMed: 18216262]
55. Guo D, Lu Z. Kinetics of inward-rectifier K+ channel block by quaternary alkylammonium ions. dimension and properties of the inner pore. J Gen Physiol 2001; 117:395–406. [PubMed: 11331349]
56. Weaver CD, Harden D, Dworetzky SI, Robertson B, Knox RJ. A thallium-sensitive, fluorescence-based assay for detecting and characterizing potassium channel modulators in mammalian cells. J Biomol Screen 2004; 9:671–7. [PubMed: 15634793]
57. Marti-Renom MA, Stuart AC, Fiser A, Sanchez R, Melo F, Sali A. Comparative protein structure modeling of genes and genomes. Annu Rev Biophys Biomol Struct 2000; 29:291–325. [PubMed: 10940251]
58. Dong E, Smith J, Heinze S, Alexander N, Meiler J. BCL::Align-sequence alignment and fold recognition with a custom scoring function online. Gene 2008; 422:41–6. [PubMed: 18601985]
59. Case DA, Cheatham TE, Darden T, Gohlke H, Luo R, Merz KM, et al. The Amber biomolecular simulation programs. J Comput Chem 2005; 26:1668–88. [PubMed: 16200636]
60. Pettersen EF, Goddard TD, Huang CC, Couch GS, Greenblatt DM, Meng EC, Ferrin TE. UCSF Chimera—a visualization system for exploratory research and analysis. J Comput Chem 2004; 25:1605–12. [PubMed: 15264254]
61. Kortemme T, Baker D. A simple physical model for binding energy hot spots in protein-protein complexes. Proc Natl Acad Sci USA 2002; 99:14116–21. [PubMed: 12381794]

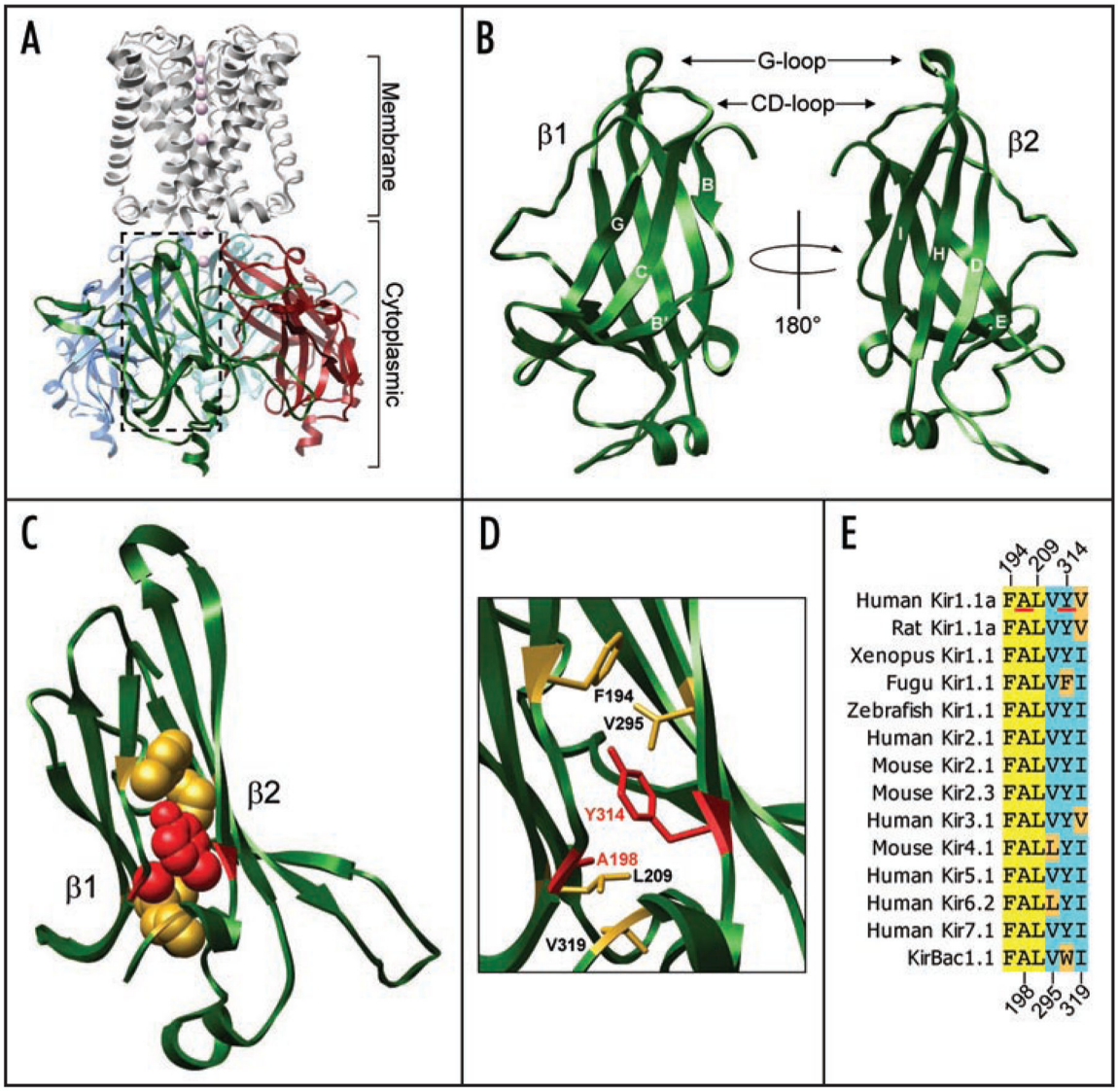

Figure 1.

The Kir1.1 channel immunoglobulin-like domain. (A) Homology model of the Kir1.1 cytoplasmic domain juxtaposed to the membrane-spanning portion of the Kir3.1-KirBac1.3 chimera. Seven K^+ ions (purple spheres) are shown in the pore. (B) The Kir1.1 immunoglobulin-like domain (IgLD) of the green subunit (A, boxed area) is shown in two orientations to highlight the β-strands comprising β_1 (left) and β_2 (right) sheets. The "G-loop" and "CD-loop" are also highlighted (see Discussion). (C) Space-filling and (D) stick model of the Kir1.1 IgLD core. Core residues mutated in Bartter syndrome (A198 and Y314) are colored red. (E) Sequence alignment of core residues from the indicated Kir channels. The numbers above and below the alignment indicate the position of residues in rat Kir1.1a.

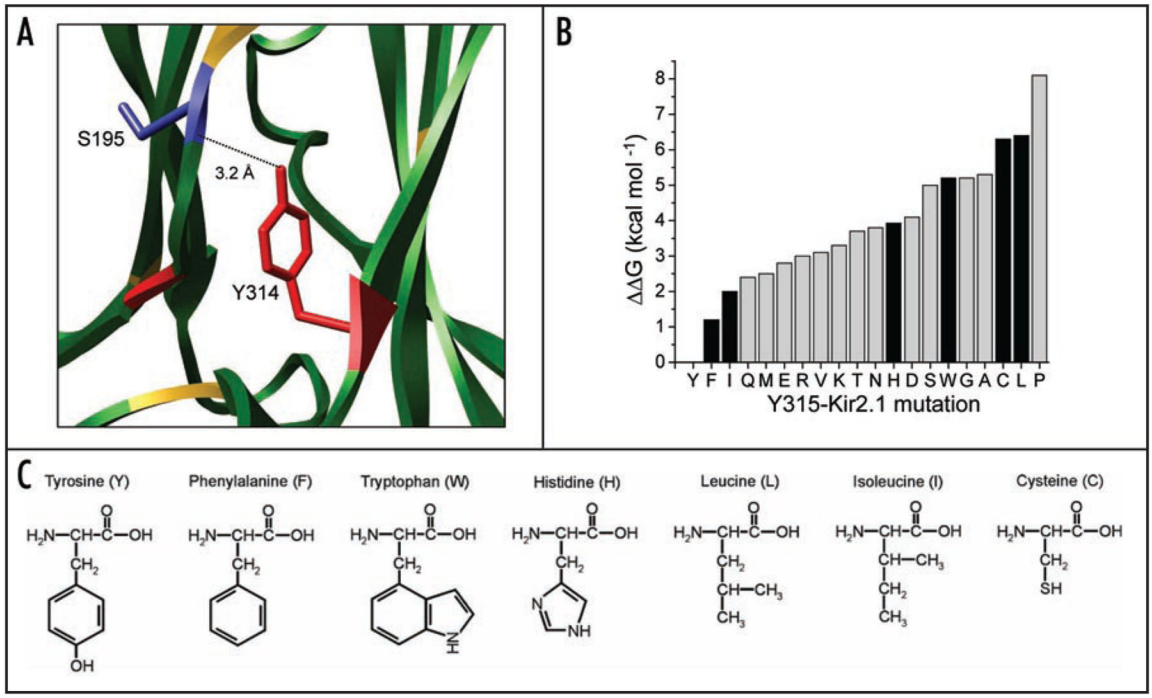

Figure 2.

Computational mutagenesis analysis of the IgLD core tyrosine residue. (A) Trans-core hydrogen bond formation between the hydroxyl group of Y314 and backbone of serine 195 in Kir1.1. (B) Tyrosine 315 of Kir2.1 was computationally mutated to all 19 other amino acids, and the resulting changes in free energy (ΔΔG) were calculated using ROSETTA. The filled black bars indicate mutations that were tested experimentally in electrophysiological and biochemical experiments. The side chain structures of these residues are shown in (C).

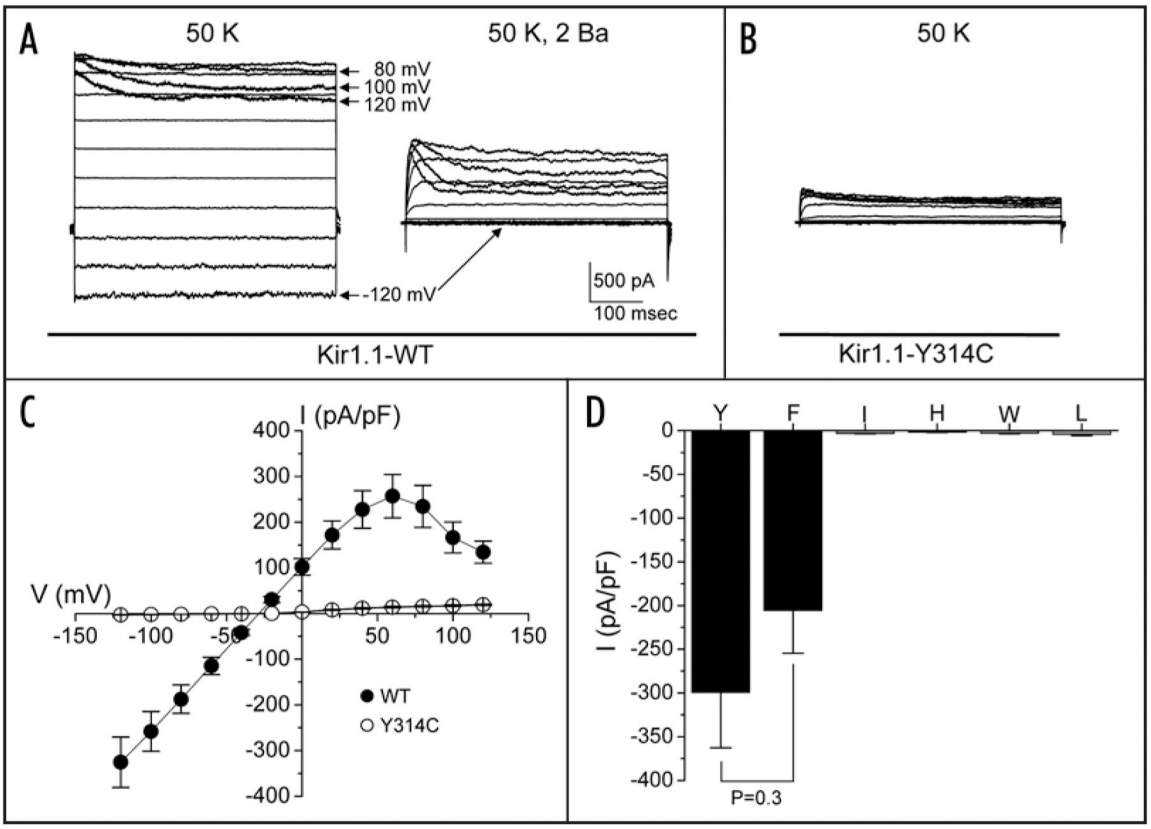

Figure 3.

Functional properties of Y314 mutants. (A) Representative WT current traces recorded in the whole-cell configuration from cells bathed in 50 mM extracellular K^+ (50 K) before (left) and after (right) bath application of 2 mM Ba^{2+} (2 Ba). Cells were voltage clamped from −120 mV to 120 mV in 20 mV increments from a holding potential of −75 mV. Note rectification of current at potentials above 80 mV (arrows). (B) Currents recorded from cells transfected with Kir1.1-Y314C in 50 mM K^+. (C) Mean ± SEM current-voltage relationships for WT (n = 9) and Y314C (n = 16) expressing cells. (D) Mean ± SEM current density recorded at −120 mV from cells expressing WT Kir1.1 (Y; n = 20) or Kir1.1 harboring the following substitutions: F (n = 13), W (n = 7), H (n = 6), L (n = 8) or I (n = 10). WT and Y314F currents were not statistically (p = 0.3) different.

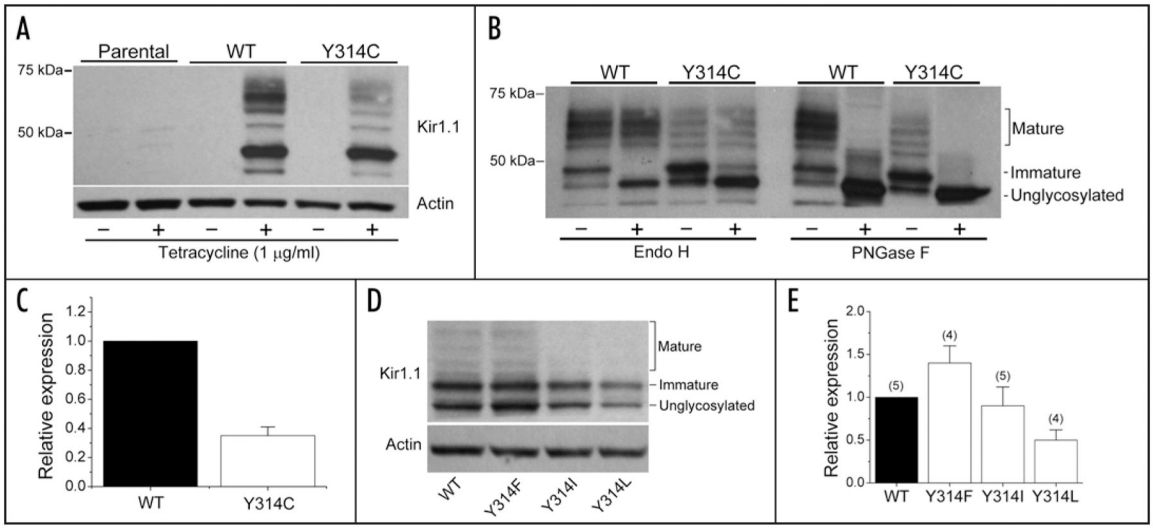

Figure 4.

Defects in Kir1.1 channel biosynthesis caused by mutations of Y314. (A) Representative Western blot of Kir1.1 expression in parental or stably transfected cell lines. Cells were cultured overnight in the absence (−) or presence (+) of Tet to induce channel expression. The membrane was stripped and re-probed for β-actin to ensure equivalent protein loading. (B) Immunoblot of whole-cell lysates from Tet-induced cells treated without (buffer control) or with Endoglycosidase H (Endo H) or Peptide N Glycosidase F (PNGase F). The figure is representative of at least 5 independent experiments. (C) Relative expression of the mature glycosylated forms of WT and Y314C-Kir1.1. The mature glycosylated bands were quantitated by densitometry and normalized to that of the WT channel. Data are means ± SEM (n = 7). (D) Representative Western blot of WT-, Y314F-, Y314I and Y314L-Kir1.1 protein expression in transiently transfected HEK-293 cells. The membrane was stripped and re-probed for actin to ensure equal protein loading. (E) Summary of 4–5 independent experiments (numbers indicated in parentheses). Data are mean ± SEM densitometry values normalized to WT-Kir1.1.

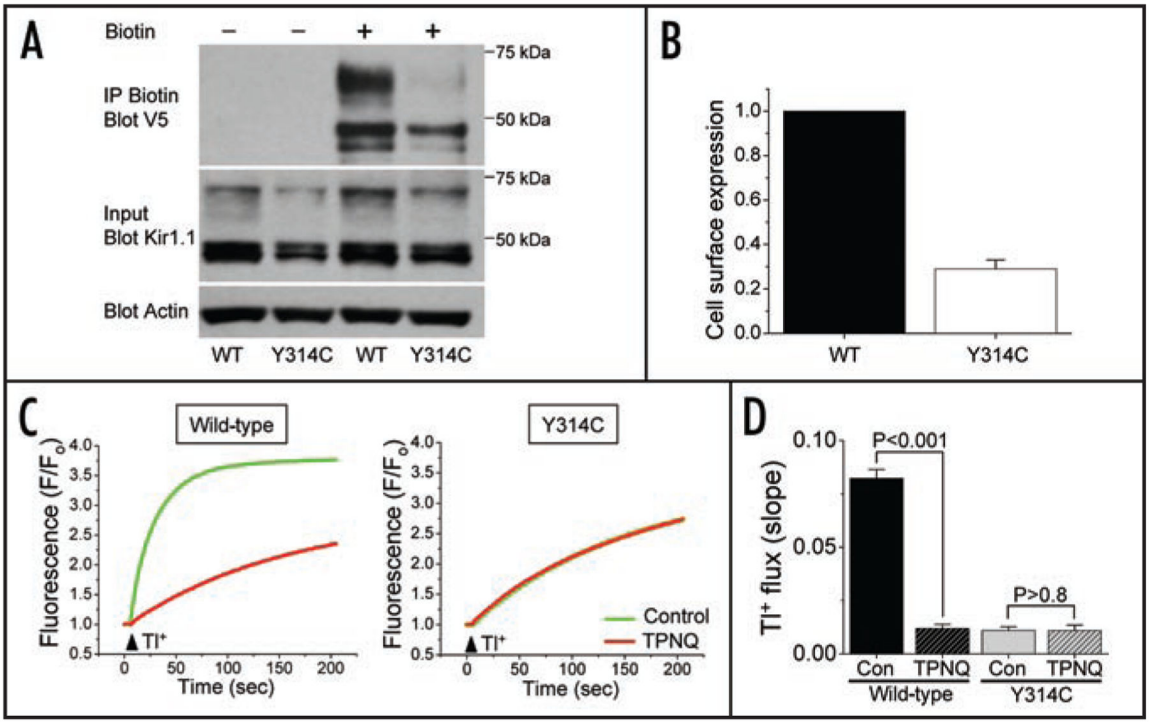

Figure 5.

Analysis of cell surface expression and function of WT and Y314C-Kir1.1. (A) Representative biotinylation experiment. HEK-293 cells stably expressing V5-tagged WT or Y314C-Kir1.1 were cultured overnight in Tet to induce channel expression. (Top) Biotinylated cell surface proteins were immunoprecipitated and subjected to immunoblot analysis using anti-V5 monoclonal antiserum. Some cells were treated without biotin (−) as a control. (Middle) Immunoblot analysis of channel expression in whole-cell lysates. (Bottom) The membrane used for whole cell lysate analysis was stripped and probed for actin to ensure equivalent protein loading. (B) Summary graph showing relative cell surface expression of WT and Y314C-Kir1.1. Biotinylated band intensity was quantitated by densitometry and normalized to that of the WT channel. Data are means ± SEM (n = 3). (C) Representative FluoZin-2 fluorescence traces recorded in the absence (green) or presence (red) of 10 μM TPNQ from Tet-induced stable cell lines expressing WT (left) or Y314C (right) Kir1.1. (D) Mean ± SEM Tl^+ flux slope values recorded from control or TPNQ-treated WT or Y314C cells between 7 and 12 seconds after Tl^+ addition (n = 16 each).

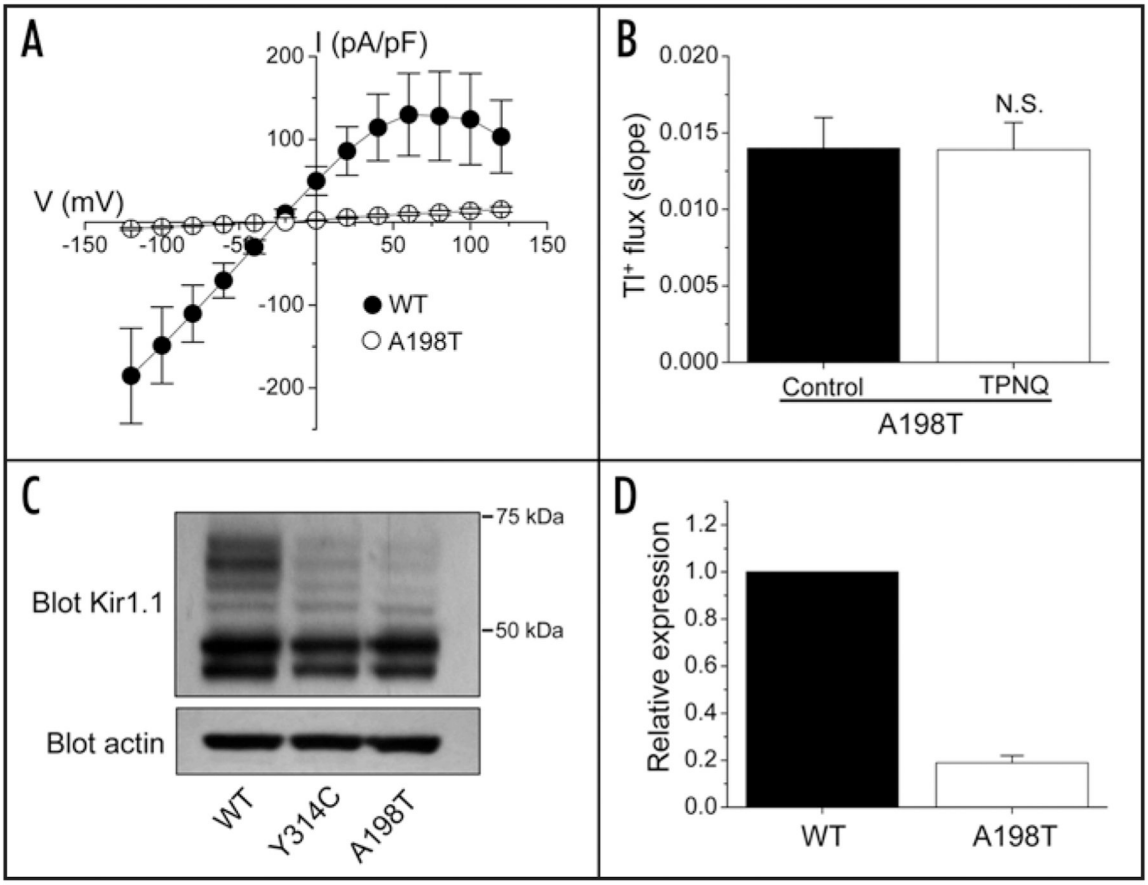

Figure 6.

Functional and biochemical properties of A198T-Kir1.1. (A) Mean ± SEM I-V relationships recorded from HEK-293 cells transiently expressing WT- or A198T-Kir1.1 (n = 5 each). (B) Mean ± SEM Tl^+ flux recorded from Tet-induced stably transfected HEK-293 cells expressing WT- or A198T-Kir1.1 (n = 16 each). Tl^+ flux assays were performed as described in Figure 5. (C) Representative immunoblot analysis of WT, Y314C and A198T stable cell lysates (top) and actin (bottom) as a loading control. (D) Summary graph showing relative whole-cell expression of WT- and A198T-Kir1.1. The mature glycosylated bands were quantitated by densitometry and normalized to that of the WT channel. Data are means ± SEM (n = 4).

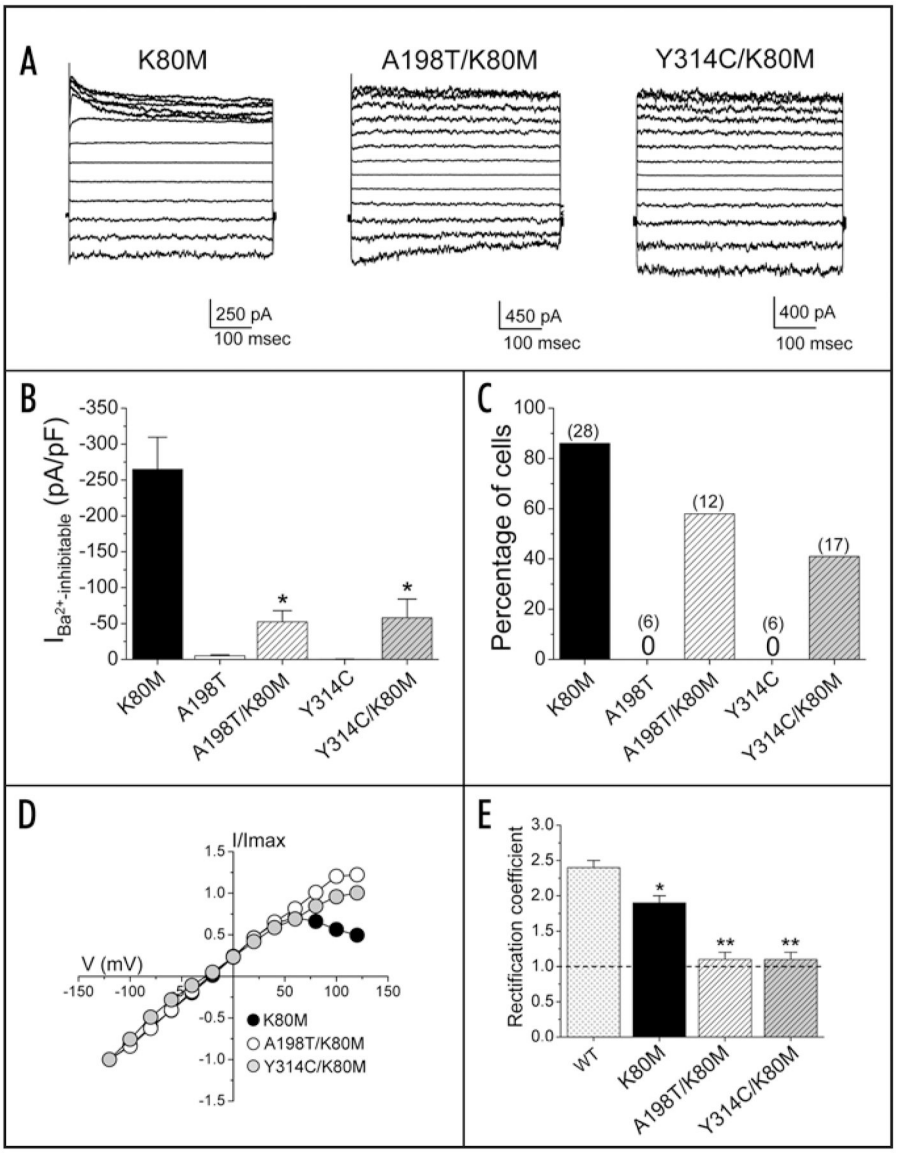

Figure 7.

Mutation of the helix-bundle gate rescues function of IgLD core mutants and reveals loss of current rectification. (A) Representative whole-cell current traces recorded between −120 mV and 120 mV from HEK-293 cells expressing K80M (left), A198T/K80M (middle) or Y314C/K80M (right). (B) Mean ± SEM Ba^{2+} (2 mM)-inhibitable current density (pA/pF) recorded at −120 mV from cells expressing K80M (n = 28), A198T (n = 6), A198T/K80M (n = 12), Y314C (n = 6) or Y314C/K80M (n = 17). *Indicates statistical difference from K80M. (C) Percentage of cells expressing greater than −10 pA/pF at −120 mV when transfected with the indicated channel cDNA. Numbers in parentheses indicate the total number of cells examined. A zero (0) indicates that no cells expressed greater than −10 pA/pF. (D) Current-voltage relationships for K80M, A198T/K80M or Y314C/K80M constructed from the representative current traces shown in (A). (E) Mean ± SEM rectification coefficients calculated from cells expressing WT (n = 27), K80M (n = 14),

A198T/K80M (n = 6) and Y314C/K80M (n = 5) Kir1.1. Rectification ratio is calculated as the absolute value of current amplitude at −120 mV divided by that recorded at 120 mV. The dashed line indicates a rectification coefficient of 1.0 (i.e., no rectification). *Statistically different ($p < 0.02$) from WT; **statistically different ($p < 0.01$) from K80M.

Table 1

Computational alanine-scanning mutagenesis of the Kir channel IgLD core

Kir1.1 residue	Kir2.1 mutation	ΔΔG (kcal mol^{-1})	% Rank
F194	F195A	4.2	94
A198	A199A	-	-
L209	L210A	3.0	88
V295	V296A	2.5	79
Y314	Y315A	4.3	94
V319	I320A	3.1	89

Amino acids in Kir2.1 (column 2) corresponding to hydrophobic core residues in Kir1.1 (column 1) were computationally mutated to alanine using ROSETTA. Mean changes in free energy (ΔΔG) calculated for each amino acid in the tretrameric channel (column 3) were rank ordered (column 4) to identify residues exhibiting the most destabilizing effect. IgLD core residues ranked at the top 88–94% of most destabilizing mutations.